SLAC-PUB-2523
May 1980
(T/E)

PARAMETERS OF THE SIX-QUARK MODEL*

Bradley D. Gaiser
Institute of Theoretical Physics, Department of Physics
Stanford University, Stanford, California 94305

Thomas Tsao and Mark B. Wise†
Stanford Linear Accelerator Center
Stanford University, Stanford, California 94305

ABSTRACT

The restrictions imposed on the parameters of the six-quark model by the neutral kaon system are discussed with QCD effects included in the leading logarithmic approximation. The dependence on the six-quark model parameters of the sign and magnitude of the CP violation parameter ε', the b-quark lifetime and the ratio of decay widths $\Gamma(b \to uX)/\Gamma(b \to cX)$ are also discussed.

(Submitted to Annals of Physics)

---

*Work supported in part by the Department of Energy, contract DE-AC03-76SF00515.

†Address beginning Sept. 1980: Dept. of Physics, Harvard University, Cambridge, MA 02138.

I. Introduction

The neutral kaon system has played an important role in elementary particle physics. The small measured value of the K_L-K_S mass difference and the near absence of a strangeness changing neutral current in kaon decays led Glashow, Iliopoulos and Maiani to propose a fourth charmed quark.[1] Later Gaillard and Lee estimated the mass of the charm quark[2] by comparing the experimental value of the K_L-K_S mass difference with the value calculated in the four-quark Weinberg-Salam model.[3] This estimate gave a value for the charm quark mass close to the value later obtained from charmonium spectroscopy.

The K°-$\bar{K}^\circ$ system is the only place where CP violation has been observed. In the Weinberg-Salam model with four quark flavors and one Higgs doublet there is no CP violation.[4] However, as was first pointed out by Kobayashi and Maskawa,[5] CP violation is possible in the six-quark model. At present there is experimental evidence for five quark flavors, the fifth b-quark, with charge -1/3, and its antiparticle are the constituents of the T family of particles. A sixth quark t, with charge 2/3, is required in the Weinberg-Salam model if the left-handed fields are to be assigned to the standard weak SU(2) doublets

$$\begin{pmatrix} u \\ d' \end{pmatrix}_L , \quad \begin{pmatrix} c \\ s' \end{pmatrix}_L , \quad \begin{pmatrix} t \\ b' \end{pmatrix}_L \quad . \tag{1}$$

The right-handed fields are assigned to SU(2) singlets. The primed fields in Eq. (1) are not mass eigenstates but are related to them by a unitary transformation. With the standard choice of quark fields this transformation has the form[5]

$$\begin{pmatrix} d' \\ s' \\ b' \end{pmatrix} = \begin{pmatrix} c_1 & -s_1c_3 & -s_1s_3 \\ s_1c_2 & c_1c_2c_3 - s_2s_3e^{i\delta} & c_1c_2s_3 + s_2c_3e^{i\delta} \\ s_1s_2 & c_1s_2c_3 - c_2s_3e^{i\delta} & c_1s_2s_3 - c_2c_3e^{i\delta} \end{pmatrix} \begin{pmatrix} d \\ s \\ b \end{pmatrix} . \qquad (2)$$

Here $s_i = \sin\theta_i$ and $c_i = \cos\theta_i$ where $i\varepsilon\{1,2,3\}$. By adjusting the phases of the quark fields, the phase δ can be moved from one location in the matrix to another; however, δ cannot be completely eliminated from the matrix. It follows that a non-zero value for the phase δ will result in CP violation. The Cabibbo-type angles θ_1, θ_2 and θ_3 are chosen to lie in the first quadrant. With this convention the quadrant of the phase δ has physical significance and cannot be specified by convention. Experimental information from beta decay give $s_1^2 \simeq 0.05$. This combined with measurements of hyperon decays give the limit $s_3 \lesssim 0.5$ on violations of universality.[6,7]

The phenomenological implications of the six-quark model for CP violation in the neutral kaon system and elsewhere have been studied by Ellis, Gaillard and Nanopoulos[8] and were found to be compatible with experiments. The constraints imposed by the measured value of the K_L-K_S mass difference and the CP violation parameter ε on the parameters θ_2, θ_3 and δ of the six-quark model have also been studied.[9,10] In these calculations the $K°$-$\overline{K}°$ mass matrix is derived from the lowest order box diagram in Fig. 1, neglecting strong interaction corrections.

The effective Hamiltonian for $\Delta S = 1$ weak nonleptonic decays is computed in the six-quark model by successively treating the W-boson, t, b and and c quarks as heavy and removing their fields from explicitly appearing in the theory.[11,12] Strong interaction effects, as described by quantum chromodynamics (QCD), are taken into account by summing the leading logarithms in these large masses using renormalization group[13] techniques. The resulting effective Hamiltonian is a sum of Wilson coefficients[14] multiplied by renormalized local four-quark operators. Diagrams with heavy quark loops, so-called Penguin-type diagrams, induce local four-quark operators with a chiral structure (V-A)⊗(V+A) into the effective Hamiltonian.[15] Although the magnitude of the coefficients of these operators is small compared with those of the (V-A)⊗(V-A) operators, it has been suggested that these operators have matrix elements for nonleptonic decays of kaons and hyperons which are greatly enhanced and that these (V-A)⊗(V+A) matrix elements make important contributions to nonleptonic decay amplitudes.[15] If this is the case, then an understanding of the $\Delta I = \frac{1}{2}$ rule is possible because the (V-A)⊗(V+A) operators are purely isospin one half. The phase δ enters the weak current through couplings of the heavy quarks. Consequently if the (V-A)⊗(V+A) operators are important for the $\Delta I = \frac{1}{2}$ rule they can contribute significantly to CP violating $K \to \pi\pi$ decay amplitudes.[16] In fact, if most of the magnitude of the $K \to \pi\pi$ (I=0) amplitude is due to the contribution of the (V-A)⊗(V+A) operators, then through a redefinition of kaon phases to comply with the phase convention that the $K \to 2\pi$ (I=0) amplitude be real, these operators make a contribution to the CP violation parameter ε' which may be large enough for upcoming experiments to detect.[17] In addition, through the redefinition of the kaon phases, the (V-A)⊗(V+A) operators can make a contribution to the CP violation parameter ε which is somewhat smaller, but still comparable to that coming from the box diagram of Fig. 1. Strong interaction corrections to the box diagram have recently been calculated[18] in the six-quark model using similar techniques. These corrections are significant for both the real and the imaginary parts of the kaon mass matrix.

In this paper we discuss the restrictions the neutral kaon system imposes on the parameters of the six-quark model, including the recently calculated strong interaction corrections to the effective Hamiltonian for $\Delta S = 1$ weak nonleptonic decays and the effective $\Delta S = 2$ Hamiltonian for K°-$\overline{K}^\circ$ mixing. Particular attention is given to the effects of the strong interaction corrections. We review the uncertainties associated with the theoretical predictions for ε and the K_L-K_S mass difference. The effects of these uncertainties on the angular constraints are also discussed. In addition, we examine how the CP violation parameter ε' and the b-quark lifetime depend on the six-quark model parameters. Upcoming experiments will attempt to measure these quantities and are likely to play an important role in testing the six-quark model as well as determining the values of its parameters.

II. The Neutral Kaon System in the Six-Quark Model

To leading order in the large W-boson t-quark, b-quark and c-quark masses the effective $|\Delta S| = 2$ Hamiltonian for K°-$\bar{K}^\circ$ mixing has the form[19]

$$
\begin{aligned}
\mathcal{H}_{\mathrm{eff}}^{|\Delta S|=2} = \frac{-G_F^2}{16\pi^2} & (\bar{s}_\alpha d_\alpha)_{V-A} (\bar{s}_\beta d_\beta)_{V-A} \\
& \times \Big[\eta_1 m_c^2 \, s_1^2 c_2^2 \, (c_1c_2c_3 - s_2s_3e^{-i\delta})^2 \\
& + \eta_2 m_t^2 s_1^2 s_2^2 \, (c_1s_2c_3 + c_2s_3e^{-i\delta})^2 \\
& + 2\, \eta_3 m_c^2 \ell n \left(\frac{m_t^2}{m_c^2}\right) s_1^2 s_2 c_2 \, (c_1c_2c_3 - s_2s_3e^{-i\delta})(c_1s_2c_3 + c_2s_3e^{-i\delta}) \Big] \\
& + \mathrm{h.c.} \quad .
\end{aligned}
\tag{3}
$$

The coefficients η_1, η_2 and η_3 have been calculated[18] in the leading logarithmic approximation and depend on the running strong interaction coupling constant α_s evaluated at the heavy mass scales and at the renormalization point mass. The matrix elements of this effective Hamiltonian are evaluated in an effective theory of strong interactions[19] with three light quark flavors u, d and s. The t, b and c quarks have been treated as heavy and their fields removed from explicitly appearing in the theory.

The kaon mass matrix element is

$$M_{12} = \langle K^\circ | H_{\mathrm{eff}}^{|\Delta S|=2} | \bar{K}^\circ \rangle \quad . \tag{4}$$

The real part of this matrix element is

$$\mathrm{ReM}_{12} = \frac{-G_F^2}{16\pi^2} \langle K^\circ | (\bar{d}_\alpha s_\alpha)_{V-A} \, (\bar{d}_\beta s_\beta)_{V-A} | \bar{K}^\circ \rangle \, (2\pi)^3$$

$$\times \Big[\eta_1 m_c^2 s_1^2 c_2^2 \Big\{ (c_1 c_2 c_3 - s_2 s_3 c_\delta)^2 - s_2^2 s_3^2 s_\delta^2 \Big\}$$

$$+ \eta_2 m_t^2 s_1^2 s_2^2 \Big\{ (c_1 s_2 c_3 + c_2 s_3 c_\delta)^2 - c_2^2 s_3^2 s_\delta^2 \Big\} \tag{5}$$

$$+ 2\eta_3 m_c^2 \ell n \left(\frac{m_t^2}{m_c^2} \right) s_1^2 c_2 s_2 \Big\{ (c_1 c_2 c_3 - s_2 s_3 c_\delta)(c_1 s_2 c_3 + c_2 s_3 c_\delta)$$

$$+ c_2 s_2 s_3^2 s_\delta^2 \Big\} \Big] \quad .$$

This is related to the difference between the K_S and K_L masses by

$$m_S - m_L \simeq 2\mathrm{ReM}_{12} \quad . \tag{6}$$

The experimental value of this mass difference,[20] $m_S - m_L = -3.52 \times 10^{-12}$ MeV, imposes a constraint on the six-quark model parameters through Eqs. (5) and (6). To proceed further we must evaluate the matrix element of the renormalized local four-quark operator $(\bar{d}_\alpha s_\alpha)_{V-A} \, (\bar{d}_\beta s_\beta)_{V-A}$ between K° and $\bar{K}^\circ$ states. This matrix element has a dependence on the renormalization point mass μ which is cancelled by the μ dependence of the coefficients η_1, η_2 and η_3 (at least when they are computed exactly). We wish to pick μ near the typical light hadronic mass scale, where simple quark-model-type estimates of the K°-$\bar{K}^\circ$ matrix element may have some validity. But we also want μ large enough so that a leading logarithmic computation of the coefficients η_1, η_2 and η_3 is sensible.

It is instructive to note that the relation

$$\langle K^\circ | (\bar{d}_\alpha s_\alpha)_{V-A} \; (\bar{d}_\beta s_\beta)_{V-A} | \bar{K}^\circ \rangle$$

$$= \sum_{\substack{\text{complete} \\ \text{set } \{n\}}} \langle K^\circ | (\bar{d}_\alpha s_\alpha)_{V-A} | n \rangle \langle n | (\bar{d}_\beta s_\beta)_{V-A} | \bar{K}^\circ \rangle \quad (7)$$

is invalid because the operator $(\bar{d}_\alpha(x) s_\alpha(x))_{V-A} \; (\bar{d}_\beta(x) s_\beta(x))_{V-A}$ — where the space-time dependence has been made explicit — requires additional subtractions to make its matrix elements finite, while $(\bar{d}_\alpha(x) s_\alpha(x))_{V-A} \; (\bar{d}_\beta(y) s_\beta(y))_{V-A}$, with $x \neq y$, does not.[21] At order α_s in the strong interactions these additional subtractions arise because of diagrams like that in Fig. 2. However, there does exist a systematic approximation procedure for the matrix element $\langle K^\circ | (\bar{d}_\alpha s_\alpha)_{V-A} \; (\bar{d}_\beta s_\beta)_{V-A} | \bar{K}^\circ \rangle$ within which Eq. (7) has some significance. In the large N_c limit,[22] where N_c is the number of colors, the diagram in Fig. 2 is suppressed by a factor of $(1/N_c)^2$ compared to the free field (no strong interactions) diagram shown in Fig. 3. Generalizing this to an arbitrary order in α_s we find that Eq. (7) is valid for the leading term in the $1/N_c$ expansion for the matrix element $\langle K^\circ | (\bar{d}_\alpha s_\alpha)_{V-A} \; (\bar{d}_\beta s_\beta)_{V-A} | \bar{K}^\circ \rangle$. Each of the matrix elements $\langle n | (\bar{d}_\beta s_\beta)_{V-A} | \bar{K}^\circ \rangle$ appearing on the right-hand side of Eq. (7), can be written as the sum of two terms. One arises from connected diagrams and the other arises from possible disconnected diagrams. To leading order in $1/N_c$ the connected piece only gets a contribution from the vacuum state $|n\rangle = |0\rangle$, while the disconnected piece only gets a contribution from the two particle state $|n\rangle = |K^\circ \bar{K}^\circ\rangle$. Therefore, to leading order in $1/N_c$, the sum on the right-hand side of Eq. (7) truncates to just two terms

$$\langle K^\circ|(\bar{d}_\alpha s_\alpha)_{V-A}\ (\bar{d}_\beta s_\beta)_{V-A}|\bar{K}^\circ\rangle$$

$$\xrightarrow[N_c \to \infty]{} \langle K^\circ|(\bar{d}_\alpha s_\alpha)_{V-A}|0\rangle\langle 0|(\bar{d}_\beta s_\beta)_{V-A}|\bar{K}^\circ\rangle$$

$$+ \langle 0|(\bar{d}_\alpha s_\alpha)_{V-A}|\bar{K}^\circ\rangle\langle K^\circ|(d_\beta s_\beta)_{V-A}|0\rangle$$

$$= 2\langle K^\circ|(\bar{d}_\alpha s_\alpha)_{V-A}|0\rangle\langle 0|(\bar{d}_\beta s_\beta)_{V-A}|\bar{K}^\circ\rangle$$

$$= \frac{f_K^2 m_K}{(2\pi)^3} \quad . \tag{8}$$

It is convenient to parameterize the K°-$\bar{K}^\circ$ matrix element in terms of a quantity B, in the following fashion:

$$\langle K^\circ|(\bar{d}_\alpha s_\alpha)_{V-A}\ (\bar{d}_\beta s_\beta)_{V-A}|\bar{K}^\circ\rangle = B(\tfrac{4}{3})\,\frac{f_K^2 m_K}{(2\pi)^3} \quad . \tag{9}$$

We have just seen that in the large N_c limit B is independent of μ and has the value $B = 3/4$. If the naive valence quark model or the vacuum insertion approximation is used to evaluate the matrix element $\langle K^0|(\bar{d}_\alpha s_\alpha)_{V-A}\ (\bar{d}_\beta s_\beta)_{V-A}|\bar{K}^0\rangle$, then $B = 1$. Shrock and Treiman performed a bag model computation of the matrix element and found $B \simeq 0.4$.[23] All the above approximations neglect the renormalization point dependence of the matrix element. However, if one of these approximations for the matrix element is used in Eq. (5), the resulting expression for the K_L-K_S mass difference will not be very sensitive to the value of the renormalization point, μ.[24] This is because η_1, η_2 and η_3 are proportional, in the leading logarithmic approximation,[18] to $[\alpha_s\ (\mu^2)]^{-2/9}$ and thus depend only weakly on the value of the renormalization point mass.

The imaginary part of the mass matrix element is

$$\mathrm{ImM}_{12} = \frac{-G_F^{\;2}}{16\pi^2} \langle K^\circ | (\bar{d}_\alpha s_\alpha)_{V-A} \, (\bar{d}_\beta s_\beta)_{V-A} | \bar{K}^\circ \rangle \; (2\pi)^3 \; 2 s_2 c_2 s_3 s_\delta$$

$$\times \, [\eta_1 m_c^2 s_1^2 \; (-c_1 c_2^2 c_3 + s_2 c_2 s_3 c_\delta) + \eta_2 m_t^2 s_1^2 \; (c_1 s_2^2 c_3 + s_2 c_2 s_3 c_\delta) \tag{10}$$

$$+ \, \eta_3 m_c^2 \ell n \; (m_t^2/m_c^2) \; s_1^2 \; (c_1 c_2^2 c_3 - c_1 s_2^2 c_3 - 2 s_2 c_2 s_3 c_\delta)] \quad .$$

Let

$$\varepsilon_m = \frac{\mathrm{ImM}_{12}}{\mathrm{ReM}_{12}} \quad , \tag{11}$$

with ReM_{12} given by Eq. (5) and ImM_{12} by Eq. (10). Note that ε_m is independent of the matrix element $\langle K^\circ | (\bar{d}_\alpha s_\alpha)_{V-A} \; (\bar{d}_\beta s_\beta)_{V-A} | \bar{K}^\circ \rangle$ because it is cancelled in the ratio given by Eq. (11). Within the standard phase convention, where the $K \to 2\pi$ (I=0) amplitude is chosen to be real (apart from final state $\pi\pi$ interactions), the imaginary part of the width transition matrix element, $\mathrm{Im}\Gamma_{12}$, is negligible compared with ImM_{12}.[25] The CP violation parameter ε, defined by[26]

$$\varepsilon \equiv \frac{i\mathrm{Im}\Gamma_{12} - \mathrm{ImM}_{12}}{(\Gamma_S - \Gamma_L)/2 + i(m_S - m_L)} \quad , \tag{12}$$

then simplifies to

$$\varepsilon \simeq \frac{1}{2\sqrt{2}} \left(\frac{\mathrm{ImM}_{12}}{\mathrm{ReM}_{12}} \right) e^{i\pi/4} \quad . \tag{13}$$

The phase, $\pi/4$, originates from the experimental relation[20] between the mass and width differences $m_S - m_L \simeq -(\Gamma_S - \Gamma_L)/2$. Equation (6) has been used to relate the mass difference between kaon eigenstates to ReM_{12}. In Eq. (13) $\mathrm{ImM}_{12}/\mathrm{ReM}_{12}$ cannot simply be replaced by ε_m because the choice of quark fields in Eq. (2) does not give a real $K \rightarrow 2\pi$ (I=0) amplitude. The effective Hamiltonian for $\Delta S = 1$ weak nonleptonic decays has been calculated[11,12] in the six-quark model by successively treating the W-boson, t-quark, b-quark and c-quark as heavy and removing their fields from explicitly appearing in the theory. The resulting effective Hamiltonian density, $\mathscr{H}^{\Delta S=1}_{\mathrm{eff}} = \sum_i C_i Q_i$, is a sum of Wilson coefficients. C_i times local four quark operators Q_i constructed out of the light u, d and s quark fields. The leading logarithms of the W-boson and heavy quark masses were summed using renormalization group techniques and contribute to the Wilson coefficients C_i. The isospin ½ operator Q_6 arises from Penguin-type diagrams and has the $(V-A)\otimes(V+A)$ chiral structure which may lead to enhanced matrix elements.[11] Let f be the fraction of the $K \rightarrow 2\pi$ (I=0) amplitude that comes from the matrix elements of Q_6. If f is large, then the $K \rightarrow 2\pi$ (I=0) amplitude has a non-negligible CP violating phase, $e^{i\xi}$, where [11]

$$\xi \simeq \frac{f\ \mathrm{ImC}_6}{\mathrm{ReC}_6} \quad . \tag{14}$$

The $K \rightarrow 2\pi$ (I=0) amplitude would be real if the strange quark field is redefined by $s \rightarrow e^{i\xi} s$, in Eq. (2). At the same time

$$\frac{\mathrm{ImM}_{12}}{\mathrm{ReM}_{12}} \rightarrow \varepsilon_m + 2\xi \quad , \tag{15}$$

so that[11]

$$\varepsilon \simeq \frac{1}{2\sqrt{2}} (\varepsilon_m + 2\xi)\, e^{i\pi/4} \quad . \tag{16}$$

The experimental value[20] $\varepsilon \simeq (2.3 \times 10^{-3})\, e^{i\pi/4}$ places a further constraint on the values of the parameters θ_2, θ_3 and δ of the six-quark model. This constraint, unlike that imposed by the K_L-K_S mass difference, does not depend on the value of the matrix element $\langle K^\circ | (\bar{d}_\alpha s_\alpha)_{V-A}\, (\bar{d}_\beta s_\beta)_{V-A} | \bar{K}^\circ \rangle$.

The CP violation parameter ε' is defined by[26]

$$\varepsilon' \equiv \frac{i}{\sqrt{2}}\, e^{i(\delta_2 - \delta_0)}\, \frac{\mathrm{Im}A_2}{A_0} \quad , \tag{17}$$

where A_0 and A_2 are the isospin zero and isospin two $K \to 2\pi$ amplitudes respectively; δ_2 and δ_0 are the $I = 2$ and $I = 0$ $\pi\pi$ phase shifts. The matrix elements of the $I = \frac{1}{2}$ operator Q_6 cannot contribute to the $I = 2$ amplitude A_2. However, by redefining the phase of the strange quark field to make the amplitude A_0 real, A_2 picks up an imaginary part. The experimental values[25] for the phase shifts δ_0 and δ_2 along with $\mathrm{Re}A_2/A_0 \approx 1/20$ yields[11]

$$\varepsilon' \simeq \frac{1}{20\sqrt{2}}\, e^{i\pi/4}\, (-\xi) \quad . \tag{18}$$

Experimentally[25] $|\varepsilon'/\varepsilon| \lesssim 1/50$; however, upcoming experiments[17] should be capable of detecting a non-zero value for ε'/ε at the fraction of a percent level.

In principle the experimental value of the K_L-K_S mass difference can be used in Eqs. (6) and (7) to determine the angle θ_2 as a function of δ and θ_3. The measured value of ε can then be used (cf. Eqs. (16), (14), (11), (10) and (5)) to determine δ as a function of θ_3. The net result is that the angles θ_2 and δ can be expressed as functions (perhaps multivalued) of the angle θ_3. In practice, there are a number of uncertainties introduced by the dependence of the theoretical expressions for $m_S - m_L$ and ε on additional parameters besides the angles θ_1, θ_2, θ_3 and δ. We need the heavy W-boson, t-quark, b-quark and c-quark masses. For the c-quark and b-quark masses[27] we use the values 1.5 GeV and 4.5 GeV derived from charmonium and upsilon spectroscopy. Since the value of the t-quark mass is presently unknown, it is treated as an additional parameter. The mass of the W-boson is taken to be 78 GeV. The QCD corrections depend on the strong interaction running coupling constant evaluated at the large W-boson, t-quark, b-quark and c-quark masses. In the leading logarithmic approximation

$$\alpha_s(Q^2) = \frac{12\pi}{33 - 2N_f} \frac{1}{\ell n(Q^2/\Lambda^2)} \quad . \tag{19}$$

We use $\Lambda^2 = 0.1\ \mathrm{GeV}^2$ and $\Lambda^2 = 0.01\ \mathrm{GeV}^2$, which are consistent with results from deep inelastic scattering.[28] When the leading logarithmic approximation is valid, the results should not be very sensitive to the precise value of Λ^2. In Eq. (19), N_f is the number of quark flavors being equal to 6, 5 and 4 at the mass scales of the t, b and c-quarks respectively. The constraints imposed by the K_L-K_S mass difference depend on the value of the matrix element $\langle K^\circ | (\bar{d}_\alpha s_\alpha)_{V-A} (\bar{d}_\beta s_\beta)_{V-A} | \bar{K}^\circ \rangle$ or equivalently, if Eq. (9) is used, on the parameter B.[29]

In Fig. 4, s_2, s_δ and ε'/ε are plotted as functions of s_3 for $s_\delta > 0$. Solutions for $s_\delta < 0$ also exist[30] and will be discussed later. For Figs. 4 we use $m_t = 30$ GeV, $B = 1$ and $f = 0.75$. The values of the quantities η_1, η_2, η_3 and C_6 are taken from Refs. 18 and 11,[31] with the renormalization point chosen so that $\alpha_s(\mu^2) = 1$. Some features of these graphs can be understood from the expressions for ReM_{12} and ImM_{12} given in Eqs. (5) and (10). While Eqs. (5) and (10) are quite complicated, a considerable simplification occurs for s_3 near zero. Treating s_3 and s_1 as small quantities we have

$$\mathrm{ReM}_{12} \propto \left\{\eta_1 m_c^2 c_2^4 + \eta_2 m_t^2 s_2^4 + 2\eta_3 m_c^2 \ln\, (m_t^2/m_c^2)\; c_2^2 s_2^2\right\} \quad , \tag{20a}$$

and

$$\mathrm{ImM}_{12} \propto 2 s_2 c_2 s_3 s_\delta \left\{-\eta_1 m_c^2 c_2^2 + \eta_2 m_t^2 s_2^2 + \eta_3 m_c^2 \ln\left(\frac{m_t^2}{m_c^2}\right)(c_2^2 - s_2^2)\right\} \quad . \tag{20b}$$

The constant of proportionality in Eqs. (20) is independent of θ_2, θ_3 and δ. For small s_3 the constraints imposed by the K_L-K_S mass difference and ε depend on δ only through its sine. Thus the sign of c_δ is irrelevant at small s_3. Note also that the K_L-K_S mass difference constraint gives a simple quadratic equation for s_2^2. This quadratic equation has at most one positive solution for s_2^2. Therefore, s_δ is a single valued hyperbolic function of s_3 in the region of small s_3. The measured value of the phase of ε implies that s_δ is positive[16] for small s_3. Away from $s_3 \approx 0$ the solutions for s_δ and s_2 become double valued and depend on the sign of c_δ. For $c_\delta < 0$, there is a cancellation between the terms which form the coefficient of m_t^2 in Eq. (5). The mass difference constraint then implies that for fixed s_3, s_2 should be larger for the case $c_\delta < 0$ than for $c_\delta > 0$. From Eq. (10) we see that ImM_{12} is proportional to $s_2 s_3 s_\delta$. The ε constraint gives rise to the opposite behavior for s_δ, i.e., larger values of s_δ occurring for $c_\delta > 0$.

The general dependence of s_2 and s_δ on Λ^2 can also be inferred from the expressions for ReM_{12} and ImM_{12} (cf. Eqs. (5) and (10)). Recall from Ref. 18 that η_2 and η_3 do not depend significantly on Λ^2; however, η_1 becomes smaller as Λ^2 decreases from 0.1 GeV^2 to 0.01 GeV^2. Thus the smaller value of Λ^2 widens the gap between the four-quark model prediction for $m_S - m_L$ and its experimental value. This results in larger values of s_2. Therefore, at a given value of s_3, s_2 increases while s_δ decreases as Λ^2 is changed from 0.1 GeV^2 to 0.01 GeV^2.

The quantity ε'/ε plotted in Fig. 4c does not depend strongly on s_3. This is because both ε' and ε are proportional to $s_2 s_3 s_\delta$ so this factor cancels out in their ratio. The principal Λ^2 dependence of ε'/ε arises from the Λ^2 dependence of ReC_6. The Wilson coefficient ReC_6 increases significantly[11] (i.e., by more than a factor of two) when Λ^2 decreases from 0.1 GeV^2 to 0.01 GeV^2. This results in a corresponding decrease in ε'/ε. Note that ε'/ε is virtually independent of the sign of c_δ. This is because both ε and ε' are proportional to the factor $s_2 s_3 s_\delta$.

The plots in Figs. 4 were calculated using B = 1 which corresponds to the valence quark model or the vacuum insertion approximation for the matrix element $\langle K^\circ | (\bar{d}_\alpha s_\alpha)_{V-A} (\bar{d}_\beta s_\beta)_{V-A} | \bar{K}^\circ \rangle$. In Figs. 5 we show s_2, s_δ and ε'/ε as functions of s_3 for the same parameters as used in Figs. 4, except that here B = 0.4. This B value corresponds to a bag model evaluation[23] of the matrix element $\langle K^\circ|(\bar{d}_\alpha s_\alpha)_{V-A}\ (\bar{d}_\beta s_\beta)_{V-A}|\bar{K}^\circ\rangle$. The smaller value of B increases the discrepancy between the four-quark model prediction and the measured value of $m_S - m_L$. This leads to generally larger values of s_2 and a diminished sensitivity to Λ^2.

Results[32] from PETRA indicate that the t-quark mass must be greater than 15 GeV. For t-quark masses less than 30 GeV, larger values of s_2 than those shown in Figs. 4 and 6 will be needed to fulfill the mass difference constraint. In turn, the measured value of ε then gives smaller values for s_δ. If the mass of the t-quark is much larger than 30 GeV, it will be necessary to include higher order terms in m_t^2/m_W^2 which have been neglected in our analysis.

In Figs. 6 we plot s_2, $|s_\delta|$ and ε'/ε as a function of s_3 for δ in the lower half plane. These solutions exist if the expression within the square brackets of Eq. (10) is negative. This occurs only for $c_\delta < 0$, when s_3 is so large that the term proportional to m_t^2 is negative and dominates the square brackets in Eq. (10). Note that s_2 and s_δ are double valued functions of s_3. At fixed s_3, the larger value of s_2 in Fig. 6a corresponds to the smaller value of $|s_\delta|$ in Fig. 6b. This is in consonance with ε being proportional to $s_2 s_3 s_\delta$.

Allowed regions of s_2 and s_δ are confined to a limited range in s_3 when $s_\delta < 0$. The size of this region depends on Λ^2. Decreasing Λ^2 will increase the magnitude of the terms not proportional to m_t^2 in the expression for $\mathrm{Im}M_{12}$ (cf. Eq. (10)) and will also decrease the magnitude of the corresponding terms in the expression for $\mathrm{Re}M_{12}$ (cf. Eq. (5)). This causes the allowed region to begin at larger values of s_3. The size of the allowed range of angles also depends on B and m_t. In order that the mass difference constraint be satisfied, a smaller value for B will require that the coefficient of m_t^2 in the square brackets of Eq. (5) be larger. Hence, regions with δ in the lower half plane will be moved to larger values of s_3 as B is decreased. For B = 0.4, there are no regions with $s_\delta < 0$ that are compatible with the universality bound, $s_3 \lesssim 0.5$. Similarly, smaller values of m_t result in smaller allowed regions than those shown in Figs. 6. This is because the coefficient of m_t^2 in the square brackets of Eqs. (5) and (10) must increase as m_t decreases, pushing these regions to larger values of s_3.

When δ lies in the upper half plane, ε'/ε is positive. As shown in Fig. 6c, ε'/ε is negative when δ lies in the lower half plane. Information on the quadrant of δ will thus be obtained if upcoming experiments measure ε'/ε. For δ in the lower half plane, only a small region of allowed values of s_2 and s_δ exists. The measurement of a negative value for ε'/ε would be extremely fortuitous, providing very stringent constraints on the parameters of the six-quark model.

In Figs. 4, 5 and 6 we use the value f = 0.75 for the fraction of the $K \to 2\pi$ (I=0) amplitude arising from the matrix elements of Q_6. The constraints imposed on the parameters of the six-quark model by the experimental values of the K_L-K_S mass difference and the CP violation parameter ε are not very sensitive to the value of f chosen. However, the predicted value of ε'/ε depends crucially on f, being proportional to it. The parameter f is strongly dependent on the renormalization point. This renormalization point dependence arises because the operator Q_6 is induced only through QCD corrections and because its Wilson coefficient receives contributions mainly from integrations over virtual momenta in the limited range $\mu^2 \lesssim p^2 \lesssim m_c^2$. We use a large value of f since this allows an understanding of the $\Delta I = \frac{1}{2}$ rule. We do not know exactly what choice of renormalization point, if any, corresponds to this value of f. It is, therefore, necessary to examine the sensitivity of our results to the value of $\alpha_s(\mu^2)$ used. As mentioned above, η_1, η_2 and η_3 depend weakly on the value of $\alpha_s(\mu^2)$. However, the quantities ImC_6 and ReC_6 both depend on $\alpha_s(\mu^2)$ and, for ReC_6 the dependence is very strong. Since our constraints on the angles θ_2, θ_3 and δ do not depend strongly on the value of ξ, the renormalization point dependence of ReC_6 does not introduce a great uncertainty in these angles. However ε' is proportional to ξ and so our predictions for ε'/ε must be interpreted very qualitatively. Several authors[12,33,34] adopt another approach to calculating ε'/ε which does not use a leading logarithmic calculation of ReC_6. Rather, they rely on an estimate of the matrix element $\langle 2\pi(I{=}0)|Q_6|K^\circ\rangle$ which is combined with the experimental value of the isospin zero amplitude A_0 and the calculated value of ImC_6 to make a prediction for ξ.[35] This approach also involves an implicit choice of μ, namely that for which the estimate of the matrix element $\langle 2\pi(I{=}0)|Q_6|K^\circ\rangle$ is valid. Predictions for ε'/ε are, however, now not as sensitive to the value of $\alpha_s(\mu^2)$ used to compute C_6, since ImC_6 is much less sensitive to variations of $\alpha_s(\mu^2)$ than ReC_6. This approach generally leads to somewhat smaller values of ε'/ε than we have found.

Finally, it is instructive to compare the QCD corrected values of s_2 and s_δ (cf. Figs. 4 and 6) with the uncorrected values. In Figs. 7 and 8, s_2 and s_δ are plotted as functions of s_3 for m_t = 30 GeV, B = 1, and f = 0 for the case of no QCD corrections.[36] In the absence of QCD corrections, the quantities η_1, η_2 and η_3 are all equal to one. Since the QCD corrected values of η_1, η_2, and η_3 are smaller than one, the mass difference constraint gives rise to smaller values of s_2 in Fig. 7a than in Fig. 4a. The ε constraint then gives rise to generally larger values of s_δ in Fig. 7b than in Fig. 4b. The allowed region of angles, for which δ lies in the lower half plane, are shown in Figs. 8. This region is about the same size as the negative s_δ region in Figs. 6 corresponding to $\Lambda^2 = 0.1$ GeV^2 but considerably larger than the $\Lambda^2 = 0.01$ GeV^2 region of negative s_δ.

III. B Meson Decays

The observation of B meson decays should soon be possible at CESR. The rates for these weak decays depend on the parameters of the six-quark model. If we view inclusive B meson decays as arising from b-quark decay, in which the light quark constituent of the meson acts only as a spectator, then the dependence of the B meson lifetime on the six-quark model parameters is easily calculated.[37] The total width for b-quark decay can be written as the sum of two terms

$$\Gamma_b = \Gamma(b \to c) + \Gamma(b \to u) \tag{21}$$

The first term arises from the diagrams in Fig. 9 and is given by

$$\begin{aligned}\Gamma(b \to c) = \frac{G_F^2\, m_b^5}{192\pi^3}\left[(c_1c_2s_3 + s_2c_3c_\delta)^2 + s_2^2c_3^2s_\delta^2\right] \\ \times\left(2f\left(\frac{m_c}{m_b}\right) + \phi(m_c,m_\tau;m_b) + 3\eta f\left(\frac{m_c}{m_b}\right)\left\{c_1^2 + s_1^2c_3^2\right\}\right. \\ \left. + 3\eta\phi(m_c,m_c;m_b)\left\{s_1^2c_2^2 + (c_1c_2c_3 - s_2s_3c_\delta)^2 + s_2^2s_3^2s_\delta^2\right\}\right) \quad .\end{aligned} \tag{22}$$

The second term in Eq. (21) arises from the diagrams in Fig. 10 and is given by

$$\begin{aligned}\Gamma(b \to u) = \frac{G_F^2\, m_b^5}{192\pi^3}\left[s_1^2s_3^2\right]\left(2 + f\left(\frac{m_\tau}{m_b}\right) + 3\eta\left\{c_1^2 + s_1^2c_3^2\right\}\right. \\ \left. + 3\eta f\left(\frac{m_c}{m_b}\right)\left\{s_1^2c_2^2 + (c_1c_2c_3 - s_2s_3c_\delta)^2 + s_2^2s_3^2s_\delta^2\right\}\right) \quad .\end{aligned} \tag{23}$$

The kinematical functions f and ϕ appearing in Eqs. (22) and (23) take into account the phase space suppression due to the non-negligible masses of the c-quark and the τ-lepton.[38] The function f(x) is given by

$$f(x) = 1 - 8x^2 + 8x^6 - x^8 - 24x^4 \ln x \quad . \tag{24}$$

The other function $\phi(m_1,m_2;m_b)$ is quite complicated, but when $m_1 = m_2$, it simplifies to

$$\phi(m,m;m_b) = g\left(\frac{2m}{m_b}\right) \tag{25}$$

where

$$\begin{aligned} g(x) = {} & (1 - \frac{7}{2}x^2 - \frac{1}{8}x^4 - \frac{3}{16}x^6)(1 - x^2)^{\frac{1}{2}} \\ & + 3x^4\left(1 - \frac{x^4}{16}\right) \ln\left(\frac{1 + \sqrt{1-x^2}}{x}\right) \; . \end{aligned} \tag{26}$$

The factor η which appears in Eqs. (22) and (23) arises because of the strong interaction corrections to the effective Hamiltonian for non-leptonic b-quark decays. This Hamiltonian is derived by a two-step process in which the W-boson and the t-quark are removed from explicitly appearing. The mechanism which gives an enhancement of the matrix elements of the (V-A)$\otimes$(V+A) four-quark operators over the matrix elements of the (V-A)$\otimes$(V-A) operators in the nonleptonic kaon and hyperon decays is expected to be absent in B-meson decays.[39] Neglecting Penguin-type diagrams and using the leading logarithmic approximation we have[40]

$$\eta = \frac{1}{3}\,(2f_+{}^2 + 1/f_+{}^4) \tag{27}$$

where

$$f_+ = \left[\frac{\alpha_s(M_W^2)}{\alpha_s(m_t^2)}\right]^{6/21} \left[\frac{\alpha_s(m_t^2)}{\alpha_s(m_b^2)}\right]^{6/23} . \tag{28}$$

In the preceding section the experimental values for the K_L-K_S mass difference and the CP violation parameter ε were used to write s_δ and s_2 as functions of s_3. Using these results $\Gamma(b \to u)$ and $\Gamma(b \to c)$ can also be expressed as functions of s_3.[41] In Figs. 11 and 12 the ratio $\Gamma(b \to u)/\Gamma(b \to c)$ and the b-quark lifetime $\tau_b = 1/\Gamma_b$ are plotted as a function of s_3.

The plots in Figs. 11 correspond to allowed values of δ in the upper half plane. When δ lies in the lower half plane it is a double-valued function of s_3. Figures 12 exhibit the same plots for this case. In Figs. 11 and 12 we use solutions for s_2 and s_δ shown in Figs. 4 and 6. Recall that the previous calculation used as parameters $m_t = 30$ GeV, $B = 1$ and $f = 0.75$. As in Section II, we choose m_c and m_b to be equal to 1.5 GeV and 4.5 GeV respectively. The partial decay widths $\Gamma(b \to u)$ and $\Gamma(b \to c)$ also depend on the τ-lepton mass which has the experimental value $m_\tau = 1.8$ GeV. However, we use $m_\tau = m_c$ since the kinematical function $\phi(m_\tau, m_c; m_b)$ simplifies for this case. This approximation has no significant effect on any of our predictions. The general features of the graphs in Figs. 11 and 12 are largely determined by the expressions in the square brackets of Eqs. (22) and (23). Taking the limit $s_3 \to 0$

in these equations reveals that for very small s_3 $\Gamma(b \to u)$ is negligible and $\Gamma(b \to c)$ is roughly proportional to s_2^2. The constant of proportionality is independent of δ so that in the small s_3 limit the b-quark lifetime is independent of the sign of c_δ. Since s_2 is larger for $\Lambda^2 = 0.01$ GeV^2 than for $\Lambda^2 = 0.1$ GeV^2 (see Fig. 4a) the b-quark lifetime is smaller for $\Lambda^2 = 0.01$ than for $\Lambda^2 = 0.1$, in the region of small s_3. Away from small s_3 the b-quark lifetime, τ_b, and the ratio $\Gamma(b \to u)/\Gamma(b \to c)$ both depend on the quadrant of δ. For $c_\delta > 0$ there is no cancellation between the two terms in the square brackets of Eq. (22) so $\Gamma(b \to c)$ grows with s_3. Note also that $\Gamma(b \to u)$ grows as s_3 increases so that the b-quark lifetime decreases as s_3 increases. However, Fig. 11a shows that for $c_\delta < 0$ and δ in the upper half plane the b-quark lifetime is not as sensitive to the value of s_3. This is because the two terms in the square brackets of Eq. (22) cancel against each other, yielding a smaller $\Gamma(b \to c)$ than when $c_\delta > 0$. Note that $\Gamma(b \to u)$ still grows with s_3 and when s_3 is near the universality bound 0.5 the ratio $\Gamma(b \to u)/\Gamma(b \to c)$ becomes larger than one. So far we have been considering δ in the upper half plane. The only allowed regions when δ lies in the lower half plane is for $c_\delta < 0$ (cf. Figs. 6). Since s_2 and s_δ are double valued functions of s_3 in this region, the b-quark lifetime and $\Gamma(b \to u)/\Gamma(b \to c)$ are also double valued functions of s_3. The upper branches in Fig. 6a correspond to the upper branches in Figs. 12a and 12b. This is because the values of s_2 and s_3 are closer to each other in the upper branches of Fig. 6a, yielding a stronger cancellation between the two terms in the square brackets of Eq. (22) and hence smaller values for $\Gamma(b \to c)$ than the lower branches of Fig. 6a give.

In Figs. 13 we plot τ_b and $\Gamma(b \to u)/\Gamma(b \to c)$ as functions of s_3 for the same choice of parameters as in Figs. 5 (i.e., $m_t = 30$ GeV, $B = 0.4$, $f = 0.75$). For a given s_3, s_2 is generally larger in Fig. 5a than in Fig. 4a; therefore the b-quark lifetime is smaller in Fig. 13a than in Fig. 10a. The general dependence of the b-quark lifetime on the mass of the t-quark can be deduced in a similar fashion. At fixed s_3, a value of m_t smaller than 30 GeV gives rise to a larger value of s_2 than is shown in Fig. 4a. Therefore, when m_t is less than 30 GeV, the b-quark lifetime will generally be smaller than shown in Fig. 11a.

It is interesting to compare the predictions shown in Figs. 11 and 12 with those of the free quark model shown in Figs. 14 (for δ in the upper half plane), where strong interaction effects are neglected. The parameter η defined in Eq. (27) is equal to one in the free quark model; the QCD corrections cause η to increase slightly. Most of the effects of the QCD corrections on the b-quark lifetime, τ_b, and the ratio of u-quark to c-quark production, $\Gamma(b \to u)/\Gamma(b \to c)$, is due to the QCD corrections to the allowed values of the six-quark model parameters θ_2, θ_3 and δ. For δ in the upper half plane, the QCD corrections tend to increase the value of s_2 (at fixed s_3) so the b-quark lifetime in Fig. 14a is generally larger than in Fig. 11a. When δ is in the lower half plane the b-quark lifetime and the ratio $\Gamma(b \to u)/\Gamma(b \to c)$ in the free quark model (i.e., no strong interactions) resemble those shown in Figs. 12 with $\Lambda^2 = 0.1\ \mathrm{GeV}^2$.

IV. Summary

In this paper we examined the constraints on parameters of the six-quark model imposed by the experimental values of the K_L-K_S mass difference and the CP violation parameter ε. Unlike previous work in which QCD effects were neglected, we have made use of calculations[11,18] where strong interaction effects are taken into account by summing the large logarithms in the W-boson, t-quark, b-quark and c-quark masses using renormalization group techniques. For the W-boson, t-quark and b-quark we have confidence in this procedure; however, treating the c-quark mass as large and using it as an expansion parameter is dubious at best. For example, in calculating the K_L-K_S mass difference, dispersive contributions were neglected[42] because they do not contribute to leading order in m_c^2. Such contributions arise when the two u-quarks in the loop of Fig. 1 bind to form a low mass hadronic state. Nevertheless, we have included strong interaction effects in a systematic way and in principle some of the higher order effects could be calculated. This is an improvement over the use of the free quark model.

The presence of many additional parameters (e.g., m_t, the matrix element $\langle K^\circ|(\bar{d}s)_{V-A}\ (\bar{d}s)_{V-A}|\bar{K}^\circ\rangle$, and Λ^2) whose values are not precisely known introduce further uncertainties in the constraints on the parameters θ_2, θ_3 and δ of the six-quark model. We have explored the effects of varying these ancillary parameters.

Using the allowed values of the six-quark model parameters θ_2, θ_3 and δ we then calculated the CP violation parameter ε', the b-quark lifetime and the ratio of u-quark production to c-quark production in b-quark decays. There exists a small region of θ_2-θ_3-δ-space for which δ lies in the lower half plane and ε'/ε is negative. Since this region for $s_\delta < 0$ is much more restrictive than for $s_\delta > 0$, a measured negative value for ε'/ε in upcoming experiments would provide very stringent limits on the six-quark model parameters.[43] Within the picture where B meson decay results from a b-quark decaying into free quarks, with the final state quarks dressing themselves into hadrons with unit probability, the b-quark lifetime is equal to the B meson lifetime. We found the b-quark lifetime to be typically from 10^{-14} sec to 3×10^{-13} sec. We also found that when $c_\delta < 0$ the ratio of u-quark to c-quark production can be greater than one at large s_3.

REFERENCES

1. S. L. Glashow, J. Iliopoulos and L. Maiani, Phys. Rev. D2 (1970), 1285.

2. M. K. Gaillard and B. W. Lee, Phys. Rev. D10 (1974), 897.

3. S. Weinberg, Phys. Rev. Lett. 19, (1967), 1264; A. Salam, in Elementary Particle Theory: Relativistic Groups and Analyticity (Nobel Symposium No. 8), edited by N. Svartholm (Almqvist and Wiksell, Stockholm, 1968), 367.

4. In the 4-quark model with additional Higgs, CP violation can occur. See, for example, S. Weinberg, Phys. Rev. Lett. 37 (1976), 657 and P. Sikivie, Phys. Lett. 65B (1976), 141.

5. M. Kobayashi and T. Maskawa, Prog. Theor. Phys. 49 (1973), 652.

6. R. E. Shrock and L. L. Wang, Phys. Rev. Lett. 41 (1978), 1692.

7. The constraints imposed on the parameters of the six-quark model by the upper limit on the decay width for $K_L \to \mu^+\mu^-$ have been discussed in: R. E. Shrock and M. B. Voloshin, Phys. Lett. 88B (1979), 192.

8. J. Ellis, M. K. Gaillard and D. V. Nanopoulos, Nucl. Phys. B109 (1976), 213.

9. V. Barger, W. F. Long and S. Pakvasa, Phys. Rev. Lett. 42 (1979), 1589.

10. R. E. Shrock, S. B. Treiman and Ling-Lie Wang, Phys. Rev. Lett. 42 (1979), 1589.

11. F. J. Gilman and M. B. Wise, Phys. Rev. D20 (1979), 2392.

12. B. Guberina and R. D. Peccei, Nucl. Phys. B163 (1980), 289.

13. M. Gell-Mann and F. Low, Phys. Rev. 95 (1954), 1300; E.C.G. Stueckelberg and A. Peterman, Helv. Phys. Acta. 26 (1953), 499; C. G. Callan, Phys. Rev. D2 (1970), 1541; K. Symanzik, Commun. Math. Phys. 18 (1970), 227.

14. K. G. Wilson, Phys. Rev. 179 (1969), 1499.

15. A. I. Vainshtein, V. I. Zakharov and M. A. Shifman, Zh. Eksp. Teor. Fiz. Pis'ma Red 22, (1975), 123 [JETP Lett. 22, (1975), 65]; M. A. Shifman, A. I. Vainshtein and V. I. Zakharov, Nucl. Phys. B120 (1977), 316 and ITEP-63, ITEP-64 (1976), unpublished.

16. F. J. Gilman and M. B. Wise, Phys. Lett. 83B (1979), 83.

17. R. Bernstein et al., Fermilab. experiment E-617.

18. F. J. Gilman and M. B. Wise, SLAC-PUB-2473 (1980) (to appear in Phys. Lett.).

19. For a detailed discussion of what is meant by an effective theory of strong interactions see Section III of: E. Witten, Nucl. Phys. B104 (1976), 445.

20. Particle Data Group, Phys. Lett. 75B (1978), 1.

21. We are grateful to K. Lane for an interesting discussion on this point.

22. For a review of the large N_c limit see: E. Witten, Nucl. Phys. B160 (1979), 57; S. Coleman, SLAC-PUB-2484 (1980).

23. R. E. Shrock and S. B. Treiman, Phys. Rev. D19 (1979), 2148.

24. If the large N_c limit or the free quark model is used for both the matrix elements $\langle K^\circ|(\bar{d}_\alpha s_\alpha)_{V-A}\,(\bar{d}_\beta s_\beta)_{V-A}|\bar{K}^\circ\rangle$ and the Wilson coefficients η_1, η_2 and η_3, then the resulting expression for the $K_L - K_S$ mass difference is independent of μ.

25. See for example, K. Kleinknecht, in: Proc. XVIIth Intern. Conf. on High Energy Physics. (London, 1974), ed. J. R. Smith (Science Research Council, Rutherford Lab., 1974), 111-123.

26. T. D. Lee and C. S. Wu, Am. Rev. Nucl. Sci. 16 (1966), 511.

27. The quantities m_c and m_t appearing in Eq. 3 are actually the running c-quark and t-quark masses. These are independent of the renormalization point μ and are most appropriately associated with spectroscopy. See Ref. 18.

28. J.G.H. Degroot et al., Phys. Lett. 82B (1979), 292; 82B (1979), 456; Z. Phys. C1 (1979), 142.

29. The constraints also depend on f_K and s_1^2. We use f_K = .159 GeV and s_1^2 = 0.0519.

30. J. S. Hagelin, Harvard University preprint, HUTP-80/A018 (1980), unpublished.

31. The values of C_6 given in Ref. 11 were calculated with M_W = 85 GeV, however, they will not differ significantly from the values of C_6 when M_W = 78 GeV is used.

32. For a review see: B. H. Wiik, DESY 79/84 (1979).

33. V. V. Prokhorov, Yad. Fiz. 30 (1979), 111.

34. J. S. Hagelin, Harvard University preprint, HUTP-80/A081 (1979), unpublished.

35. The quantity ξ can also be written as $\xi \approx \left[\frac{\mathrm{Im}C_6 \langle\pi\pi(I=0)|Q_6|K^\circ\rangle}{A_o e^{i\delta_o}}\right]$.

36. The free quark model results are quite sensitive to the value of s_1^2 used. For example, if s_1^2 = 0.059 is used solutions with δ in the upper half plane would not exist for arbitrarily small s_3.

37. A similar picture when applied to D meson decays makes the unsuccessful prediction $\tau(D^o) = \tau(D^+)$. A possible explanation for the observed difference in lifetimes relies on a prominent role for the spectator in D^o decays. If this is the case, then we would expect our predictions to work only for charged B decays. See: M. Bander, D. Silverman and A. Soni, Phys. Rev. Lett. 44 (1980), 7.

38. See, for example, H. Harari, SLAC-PUB-2234 (1978), unpublished.

39. L. F. Abbott, P. Sikivie and M. B. Wise, Phys. Rev. D21 (1980), 768.

40. See, for example, A. Ali, J. G. Körner and G. Kramer, Z. Phys. C1 (1979), 269.

41. Similar discussions of b-quark decays in the six-quark model are given in Refs. 9, 10, and in: H. Harari, SLAC-PUB-2234 (1978) (unpublished); V. Barger, W. F. Long and S. Pakvasa, J. Phys. G5 (1979), L147.

42. Such contributions are discussed in: L. Wolfenstein, Nucl. Phys. B160 (1979), 501. Including these contributions would act much like a change in the parameter B.

43. If the parameter f is negative then ε'/ε will be negative for δ in the upper half plane. However, in this case the Penguin-type diagrams do not help explain the $\Delta I=1/2$ rule but rather act to suppress the $\Delta I=1/2$ enhancement.

FIGURE CAPTIONS

Fig. 1: Box diagram contributing to K°-$\overline{K}^\circ$ mixing in the six-quark model.

Fig. 2: Order α_s correction to the matrix element $\langle K^\circ | (\bar{d}_\alpha s_\alpha)_{V-A} (\bar{d}_\beta s_\beta)_{V-A} | \overline{K}^\circ \rangle$, which vanishes in the large N_c limit. The black box denotes the action of the local four-quark operator $(\bar{d}s)_{V-A} (\bar{d}s)_{V-A}$.

Fig. 3: Lowest order contribution to the matrix element $\langle K^\circ | (\bar{d}_\alpha s_\alpha)_{V-A} (\bar{d}_\beta s_\beta)_{V-A} | \overline{K}^\circ \rangle$. The black box denotes the action of the local four-quark operator $(\bar{d}s)_{V-A} (\bar{d}s)_{V-A}$. Here α and β denote the color quantum number carried by a quark line, where $\alpha,\beta \varepsilon \{1,2,3\}$.

Fig. 4: Graphs of (a) s_2, (b) s_δ and (c) ε'/ε as functions of s_3 when δ lies in the upper half plane. The parameters m_t = 30 GeV, B = 1 and f = 0.75 are used. Dashed lines are for $\Lambda^2 = 0.1$ GeV^2 and solid lines are for $\Lambda^2 = 0.01$ GeV^2. ε'/ε has almost the same value (to within 10%) for $c_\delta < 0$ and $c_\delta > 0$.

Fig. 5: Graphs of (a) s_2, (b) s_δ and (c) ε'/ε as functions of s_3 when δ lies in the upper half plane. The parameters m_t = 30 GeV, B = 0.4 and f = 0.75 are used. Dashed lines are for $\Lambda^2 = 0.1$ GeV^2 and solid lines are for $\Lambda^2 = 0.01$ GeV^2. ε'/ε has almost the same value (to within 10%) for $c_\delta < 0$ and $c_\delta > 0$.

Fig. 6: Graphs of (a) s_2, (b) $|s_\delta|$ and (c) ε'/ε as functions of s_3 when δ lies in the lower half plane. The parameters m_t = 30 GeV, B = 1.0 and f = 0.75 are used. Dashed lines are for $\Lambda^2 = 0.1$ GeV^2 and solid lines are for $\Lambda^2 = 0.01$ GeV^2. Note these regions exist only for $c_\delta < 0$.

Fig. 7: Graphs of (a) s_2 and (b) s_δ as functions of s_3, for δ in the upper half plane, in the free quark model (i.e., no strong interactions). The parameters m_t = 30 GeV and B = 1.0 are used. In the absence of strong interactions f = 0 and $\varepsilon'/\varepsilon = 0$.

Fig. 8: Graphs of (a) s_2 and (b) $|s_\delta|$ as functions of s_3, for δ in the lower half plane, in the free quark model (i.e., no strong interactions). The parameters m_t = 30 GeV and B = 1.0 and f = 0 are used.

Fig. 9: Diagram illustrating decays which contribute to the partial decay width $\Gamma(b \to c)$. The unlabeled final state fermions are: $e\,\bar{\nu}_e$, $\mu\,\bar{\nu}_\mu$, $\tau\,\bar{\nu}_\tau$, $d\,\bar{u}$, $s\,\bar{u}$, $d\,\bar{c}$, and $s\,\bar{c}$. The black box represents a local four-fermion vertex.

Fig. 10: Diagram illustrating decays which contribute to the partial decay width $\Gamma(b \to u)$. The unlabeled final state fermions are $e\,\bar{\nu}_e$, $\mu\,\bar{\nu}_\mu$, $\tau\,\bar{\nu}_\tau$, $d\,\bar{u}$, $s\,\bar{u}$, $d\,\bar{c}$, and $s\,\bar{c}$. The black box represents a local four-fermion vertex.

Fig. 11: Plot of (a) the b-quark lifetime τ_b (in seconds) and (b) the ratio of u-quark production to c-quark production $\Gamma(b \to u)/\Gamma(b \to c)$ for the allowed valves of the six-quark model parameters shown in Figs. 4a and 4b. Dashed lines are for $\Lambda^2 = .1\ \mathrm{GeV}^2$ and solid lines are for $\Lambda^2 = .01\ \mathrm{GeV}^2$.

Fig. 12: Plot of (a) the b-quark lifetime τ_b (in seconds) and (b) the ratio of u-quark production to c-quark production $\Gamma(b \to u)/\Gamma(b \to c)$ for the allowed values of the six-quark model parameters shown in Figs. 6a and 6b. Dashed lines are for $\Lambda^2 = .1\ \mathrm{GeV}^2$ and solid lines are for $\Lambda^2 = .01\ \mathrm{GeV}^2$.

Fig. 13: Plot of (a) the b-quark lifetime τ_b (in seconds) and (b) the ratio of u-quark production to c-quark production $\Gamma(b \to u)/\Gamma(b \to c)$ for the allowed values of the six-quark model parameters shown in Figs. 5a and 5b. Dashed lines are for $\Lambda^2 = .1\ \mathrm{GeV}^2$ and solid lines are for $\Lambda^2 = .01\ \mathrm{GeV}^2$.

Fig. 14: Plot of (a) the b-quark lifetime τ_b (in seconds) and (b) the ratio of u-quark production to c-quark production $\Gamma(b \to u)/\Gamma(b \to c)$ for the values of the six-quark model parameters shown in Figs. 7a and 7b.

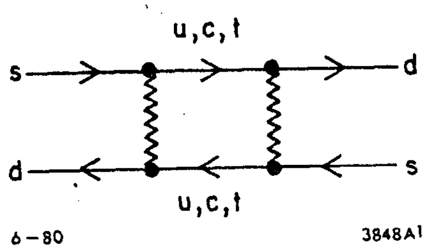

Fig. 1

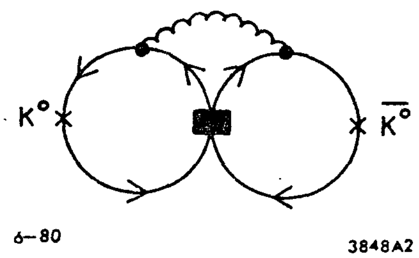

Fig. 2

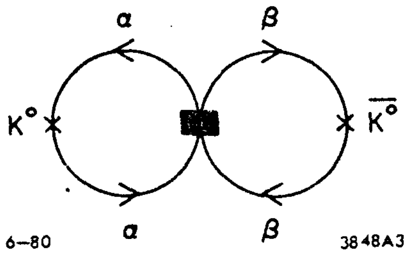

Fig 3

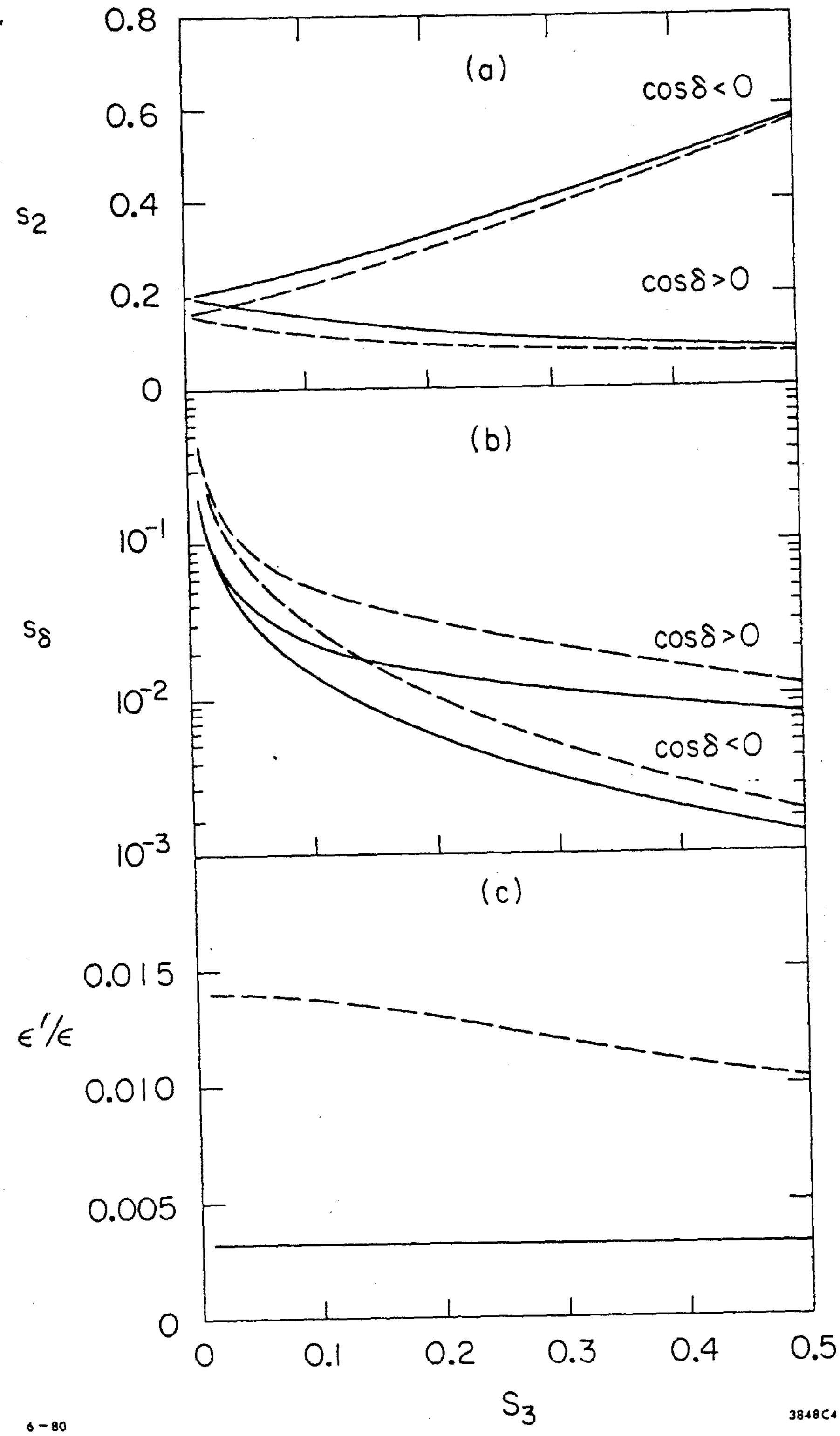
(a)
cosδ<0
cosδ>0
s_2
0.8
0.6
0.4
0.2
0
(b)
s_δ
10^{-1}
10^{-2}
10^{-3}
cosδ>0
cosδ<0
(c)
ϵ'/ϵ
0.015
0.010
0.005
0
0
0.1
0.2
0.3
0.4
0.5
S_3
6-80
3848C4

Fig. 4

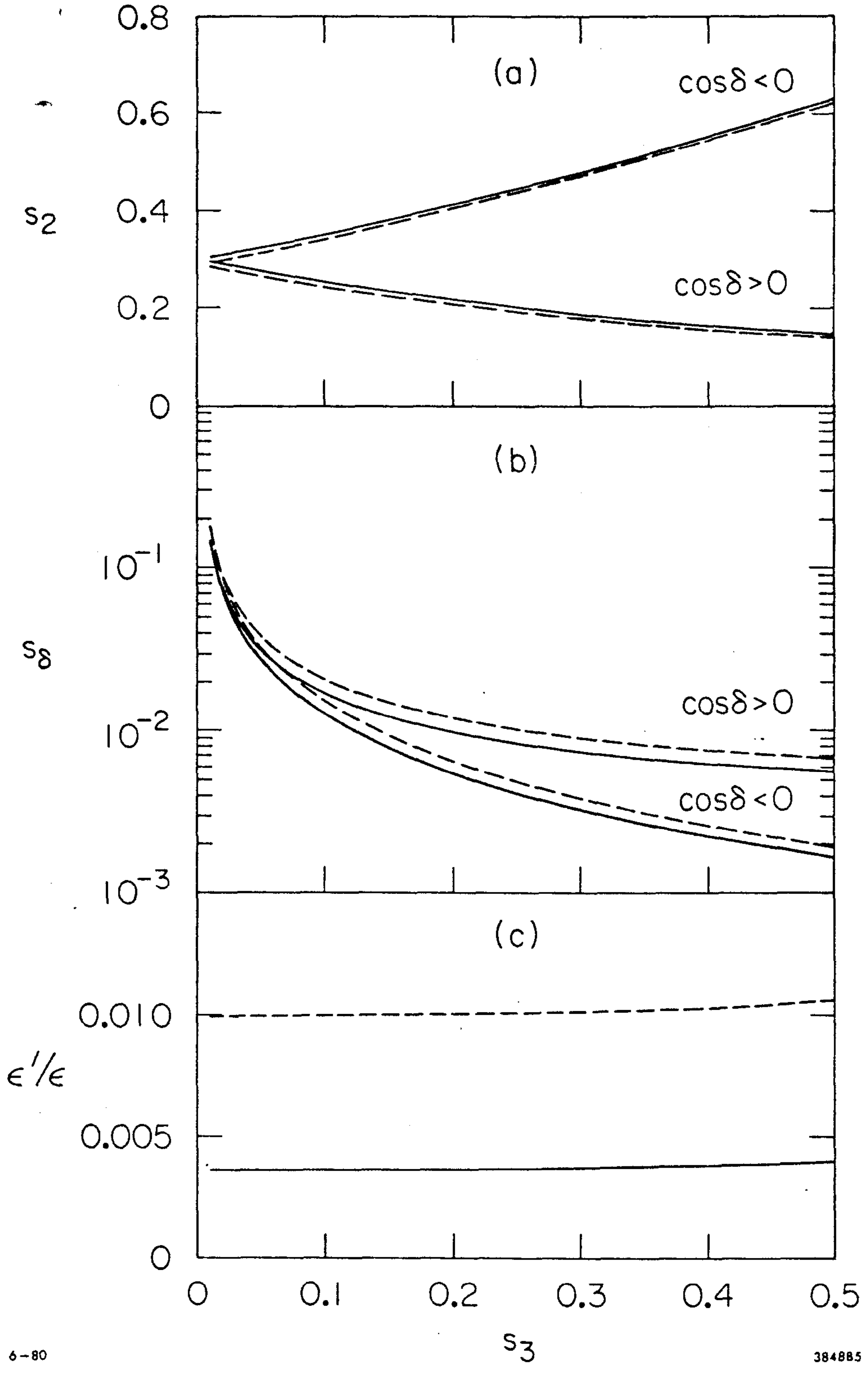

(a)
cosδ<0
cosδ>0
0.8
0.6
0.4
0.2
0
s_2
(b)
10^{-1}
10^{-2}
10^{-3}
s_δ
cosδ>0
cosδ<0
(c)
0.010
0.005
0
ϵ'/ϵ
0
0.1
0.2
0.3
0.4
0.5
s_3
6-80
384885

Fig. 5

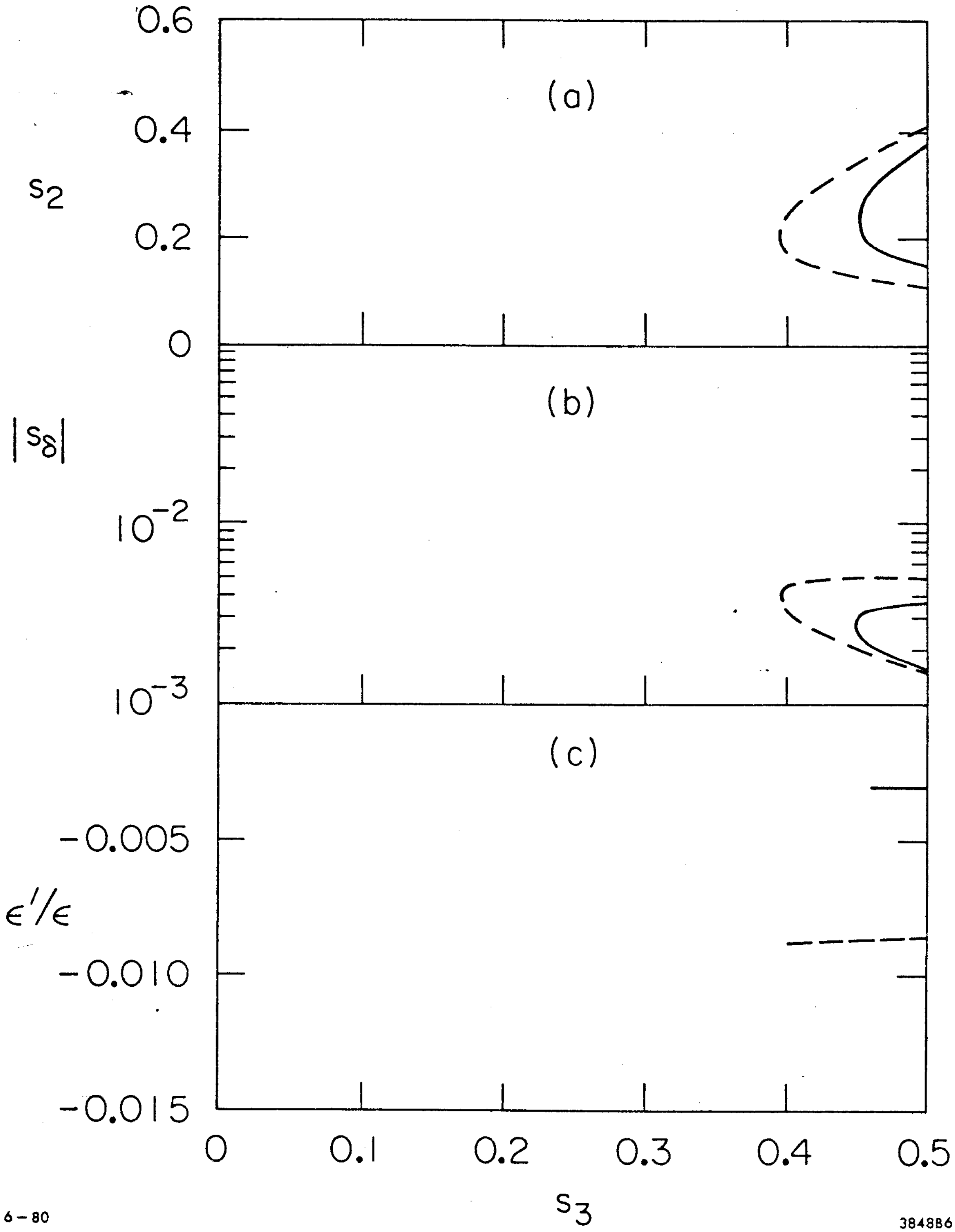
(a)
(b)
(c)
0.6
0.4
0.2
0
s_2
$|s_\delta|$
10^{-2}
10^{-3}
-0.005
-0.010
-0.015
ϵ'/ϵ
0
0.1
0.2
0.3
0.4
0.5
s_3
6-80
384886

Fig. 6

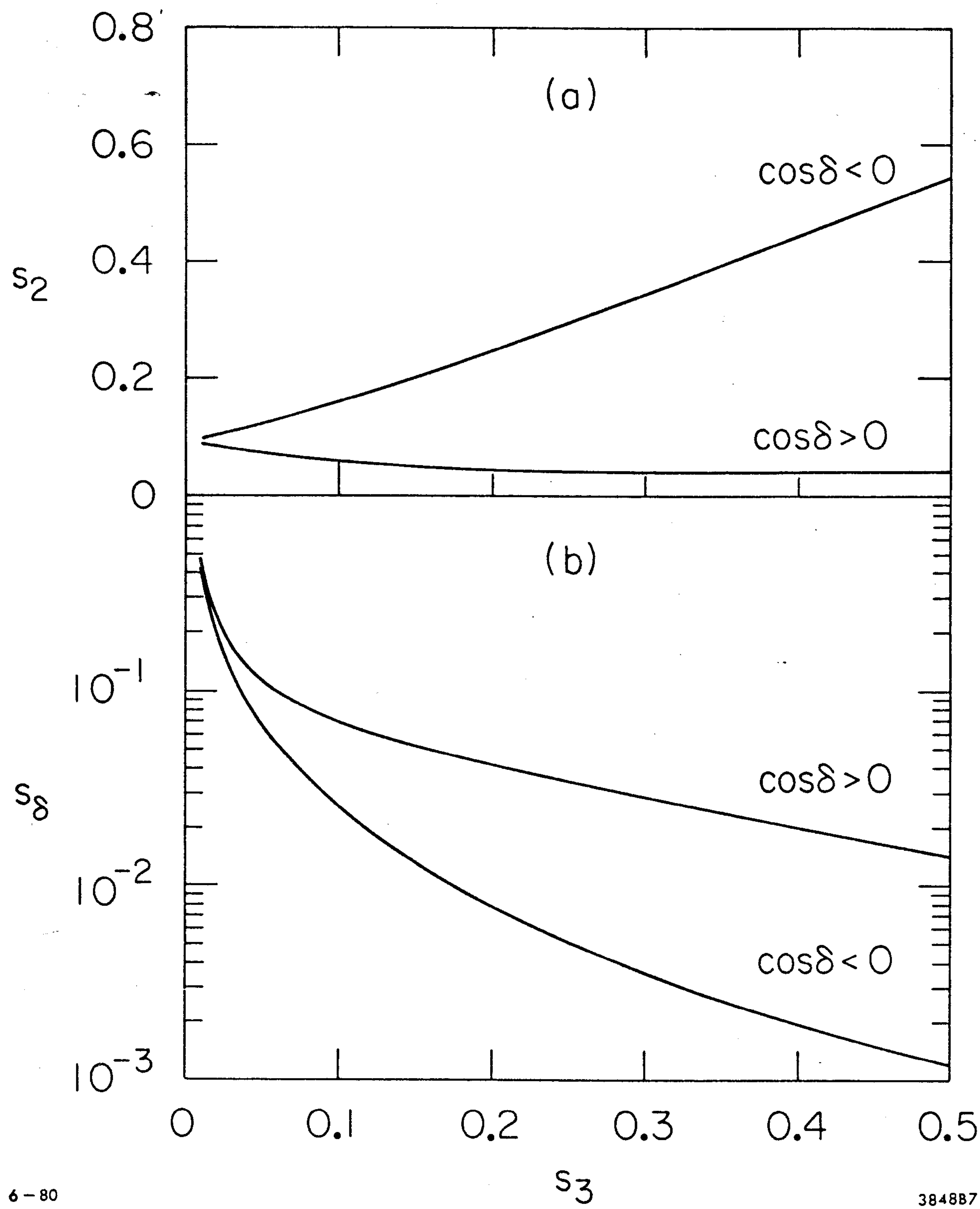

0.8
0.6
0.4
0.2
0
s_2
(a)
cosδ < 0
cosδ > 0
(b)
10^{-1}
10^{-2}
10^{-3}
s_δ
cosδ > 0
cosδ < 0
0
0.1
0.2
0.3
0.4
0.5
s_3
6 – 80
3848B7

Fig. 7

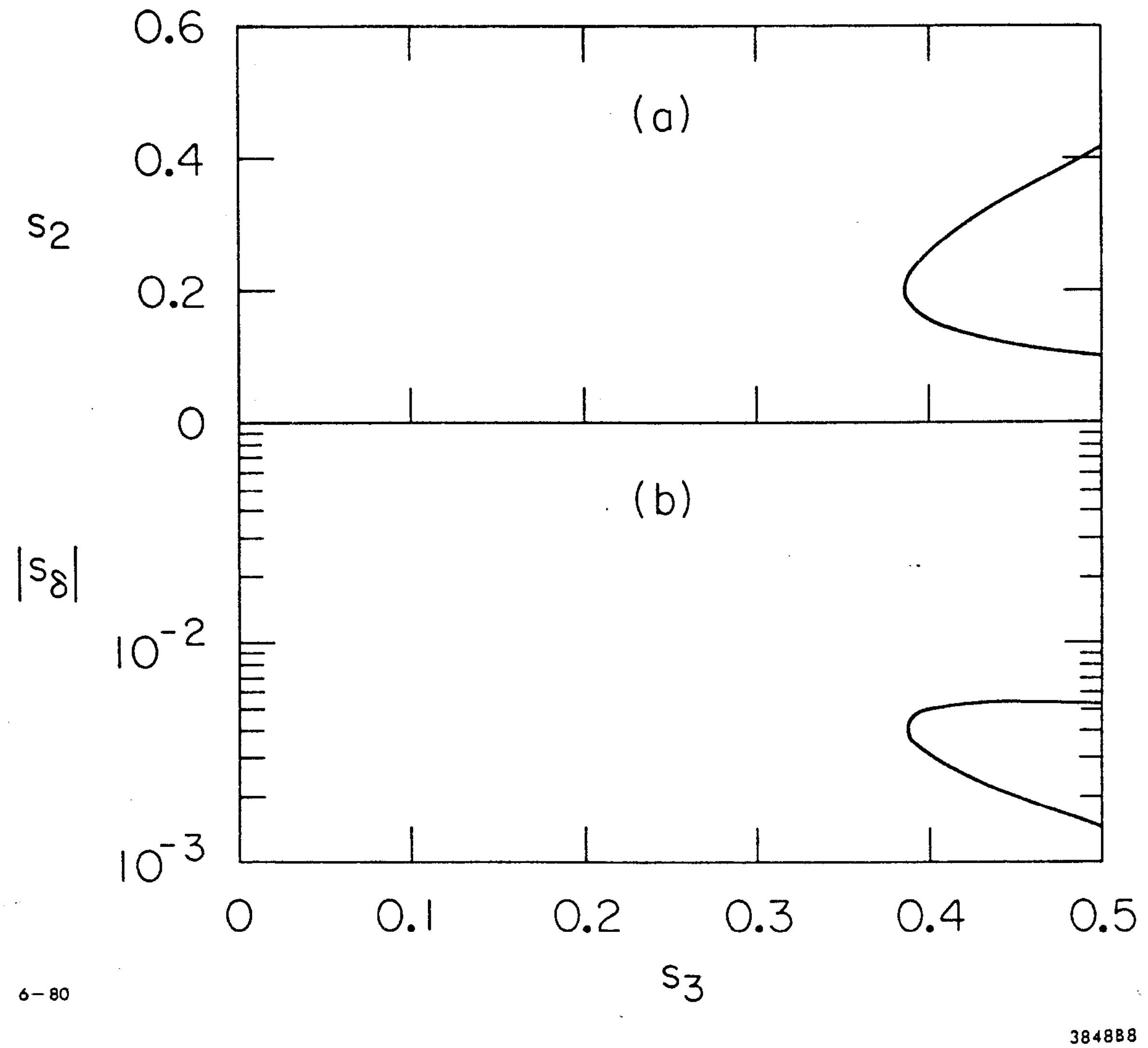

Fig. 8

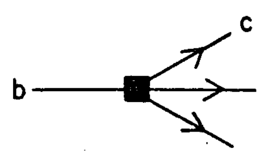

6–80 3848A9

Fig. 9

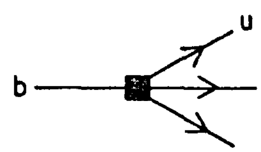

6–80 3848A10

Fig. 10

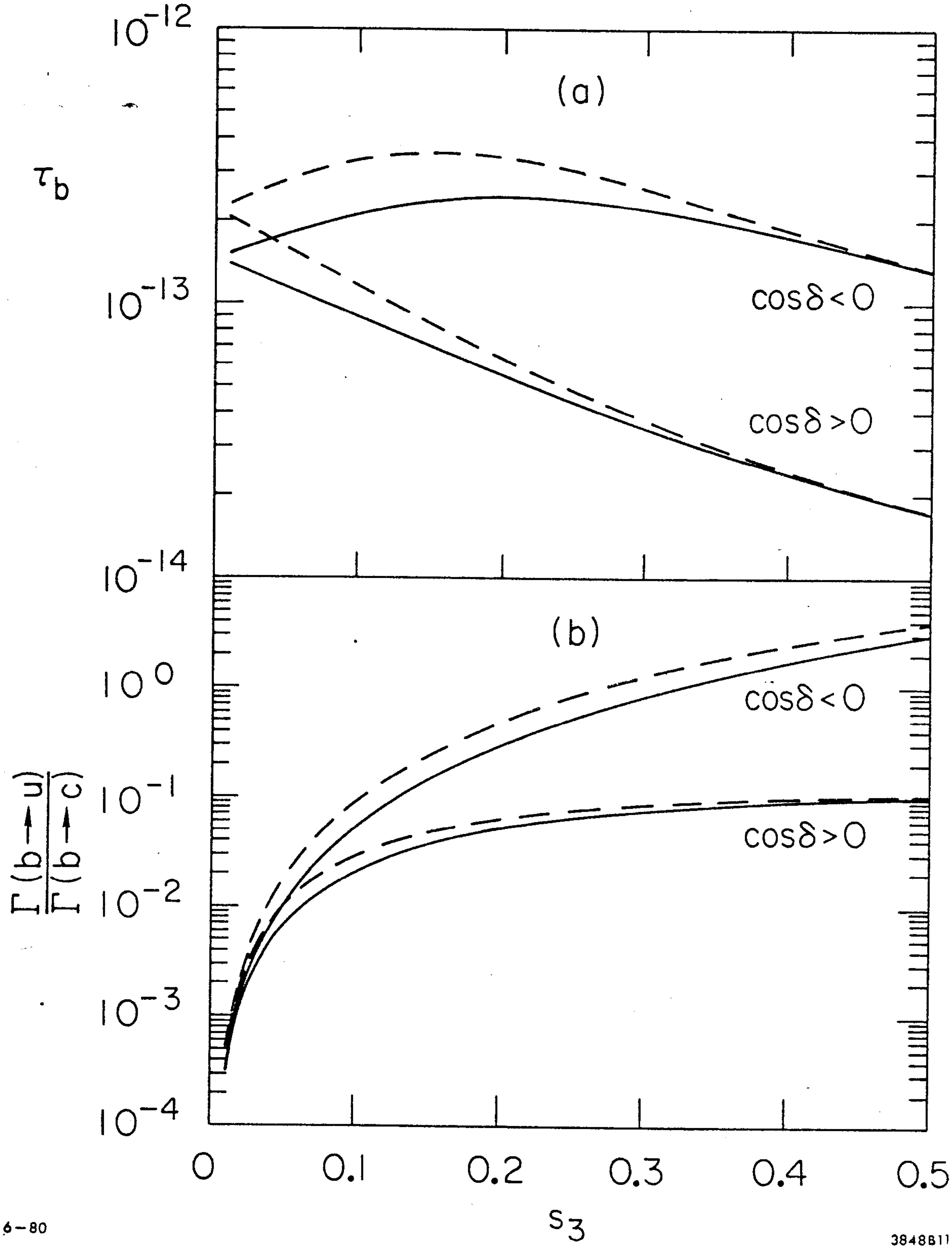

10^{-12}
(a)
τ_b
10^{-13}
cosδ<0
cosδ>0
10^{-14}
(b)
10^0
cosδ<0
10^{-1}
cosδ>0
$\frac{\Gamma(b \to u)}{\Gamma(b \to c)}$
10^{-2}
10^{-3}
10^{-4}
0
0.1
0.2
0.3
0.4
0.5
s_3
6-80
3848B11

Fig. 11

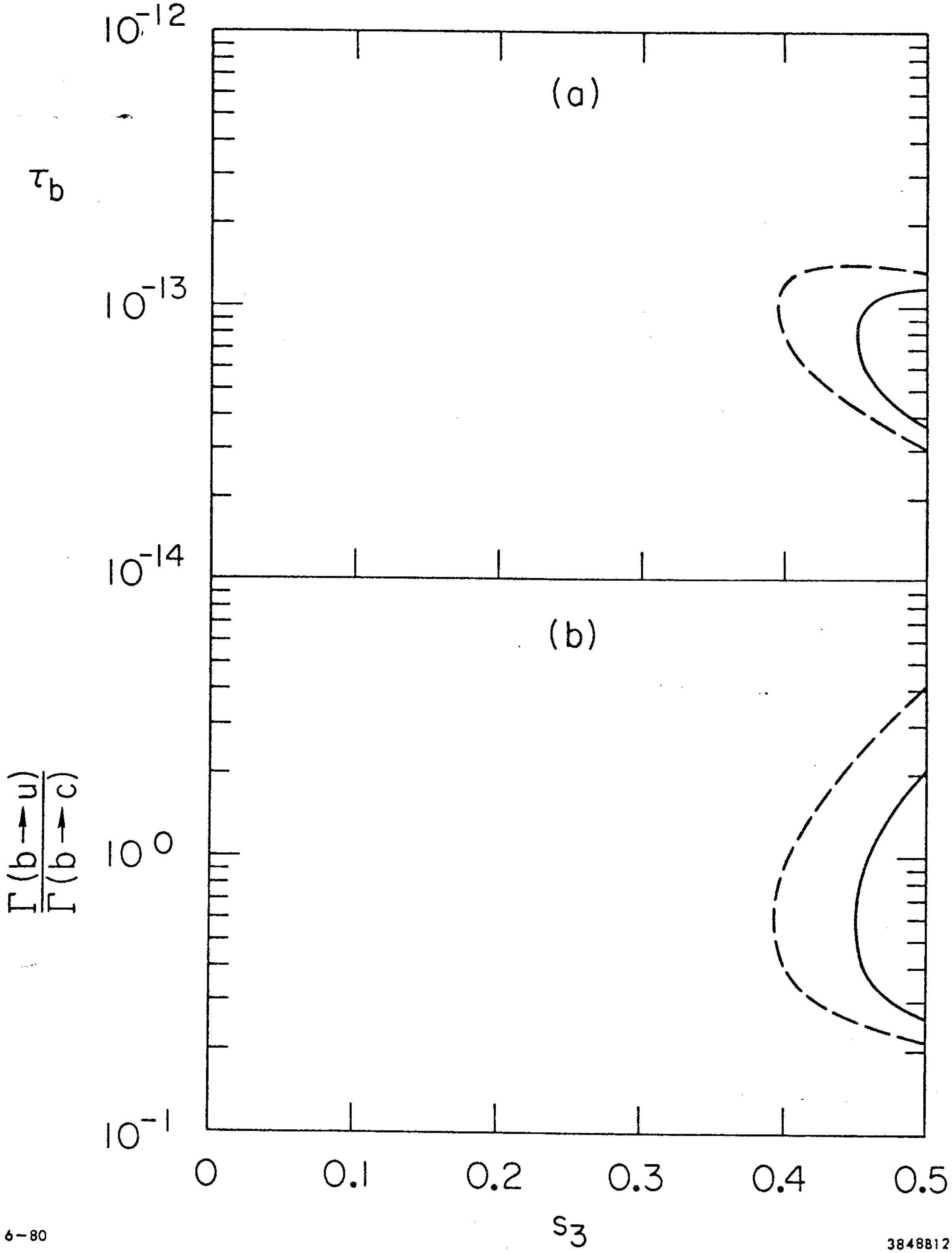
(a)
(b)
τ_b
10^{-12}
10^{-13}
10^{-14}
$\frac{\Gamma(b \to u)}{\Gamma(b \to c)}$
10^0
10^{-1}
0
0.1
0.2
0.3
0.4
0.5
s_3
6–80
3848B12

Fig. 12

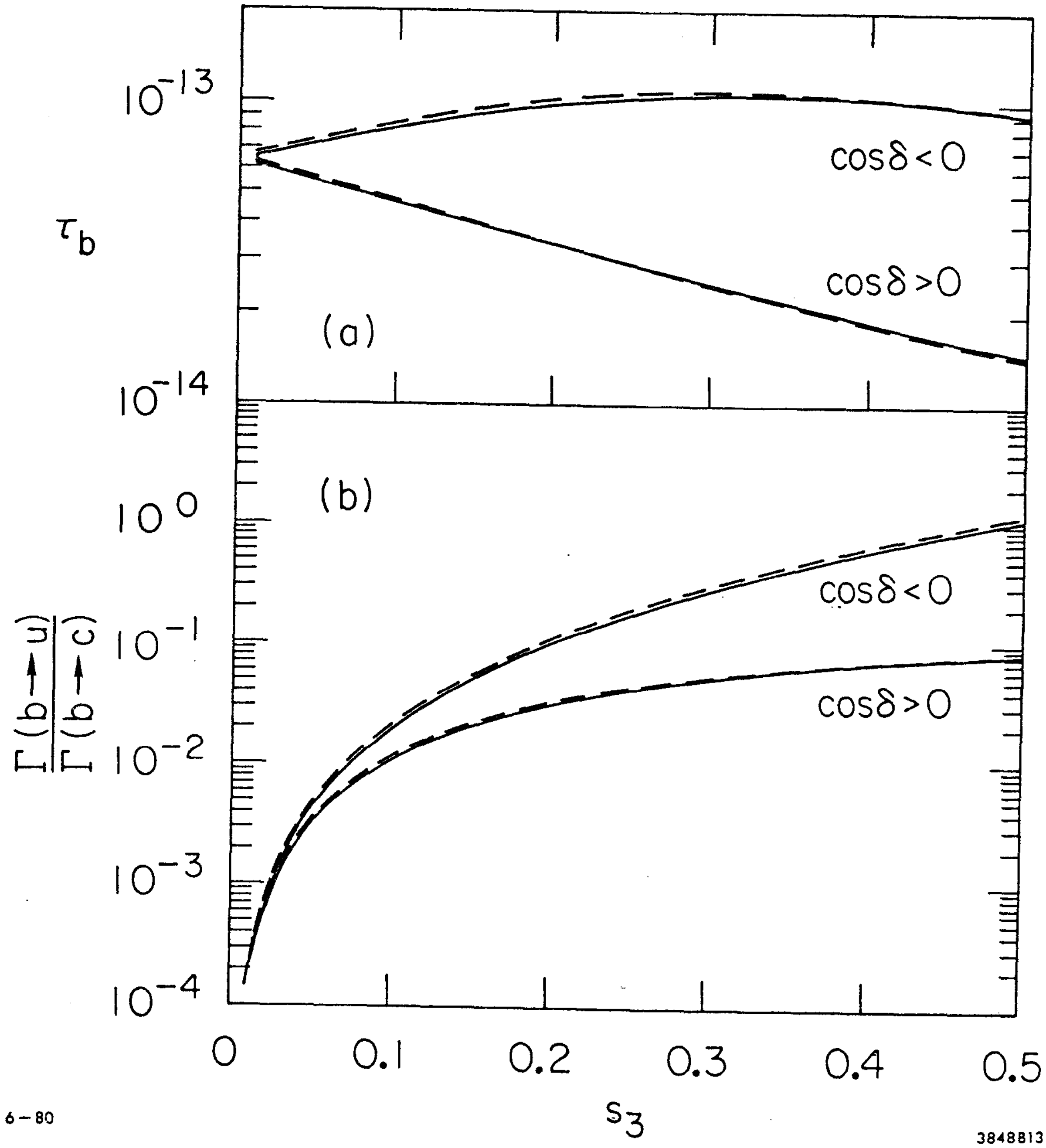

10^{-13}
τ_b
$\cos\delta<0$
$\cos\delta>0$
(a)
10^{-14}
(b)
10^{0}
$\frac{\Gamma(b\to u)}{\Gamma(b\to c)}$
10^{-1}
10^{-2}
10^{-3}
10^{-4}
$\cos\delta<0$
$\cos\delta>0$
0
0.1
0.2
0.3
0.4
0.5
s_3
6-80
3848B13

Fig. 13

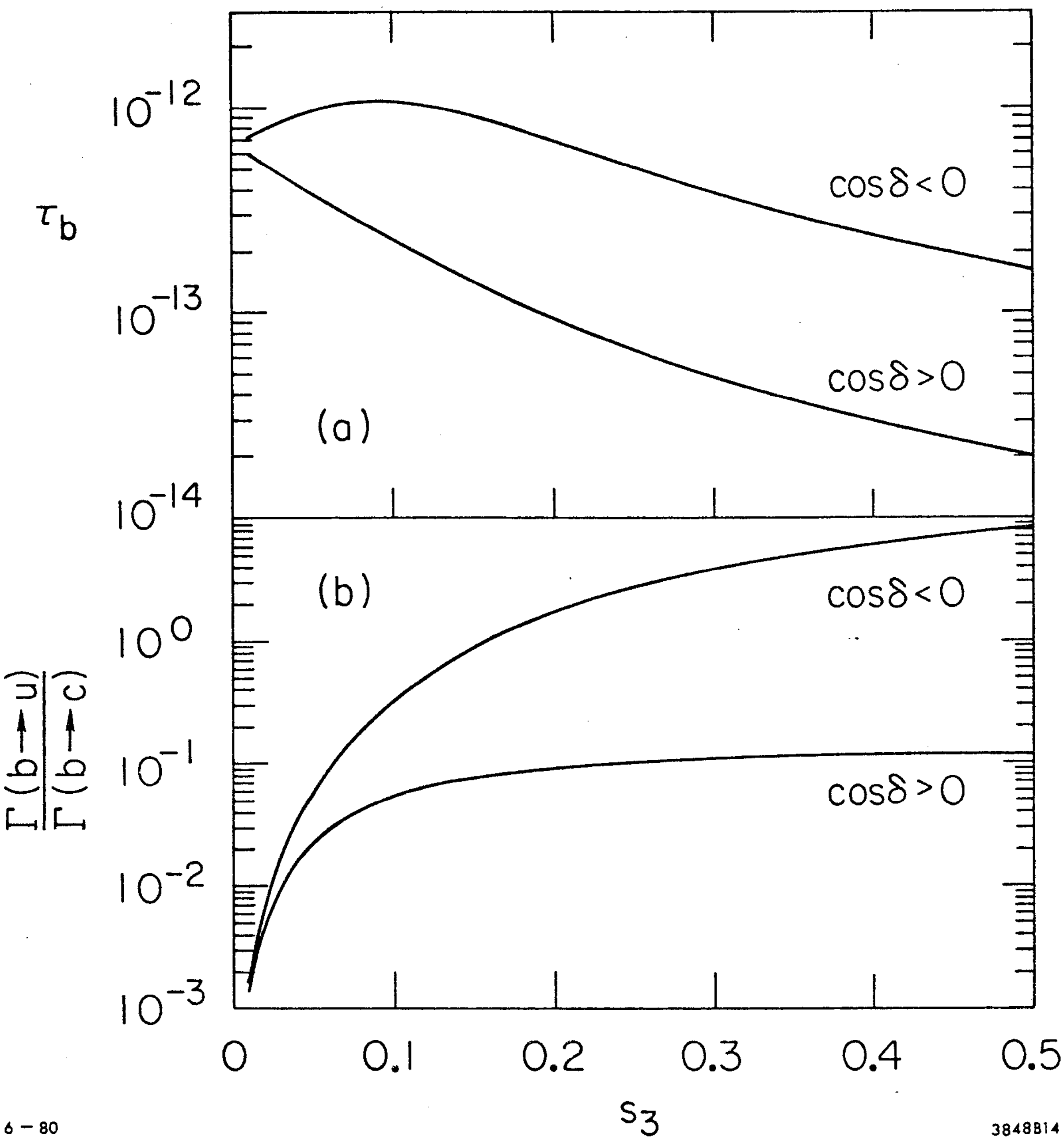

10^{-12}
10^{-13}
10^{-14}
τ_b
$\cos\delta < 0$
$\cos\delta > 0$
(a)
(b)
10^{0}
10^{-1}
10^{-2}
10^{-3}
$\frac{\Gamma(b \to u)}{\Gamma(b \to c)}$
0
0.1
0.2
0.3
0.4
0.5
s_3
6 – 80
3848B14

Fig. 14